REDOX REPORT
2025, VOL. 30, NO. 1, 2485666
https://doi.org/10.1080/13510002.2025.2485666

Taylor & Francis
Taylor & Francis Group

Spermidine prevents iron overload-induced impaired bone mass by activating SIRT1/SOD2 signaling in senile rat model

Zhi-Qing Du[a], Jia-Bin Xie[a], Sheng-Yi Ji[a], Wanshu Zhou[c] and Zhou-Shan Tao [a,b]

[a]Department of Orthopedics, The First Affiliated Hospital of Wannan Medical College, Wuhu, People's Republic of China; [b]Anhui Province Key Laboratory of Non-coding RNA Basic and Clinical Transformation, Wuhu, People's Republic of China; [c]Department of Gerontology, The Second Affiliated Hospital of Wannan Medical College, Wuhu City, People's Republic of China

ABSTRACT

Spermidine (SPD) is an organic compound known for its powerful antioxidant stress and anti-aging properties, and whether SPD has the ability to reduce bone mass in elderly iron overload rats is unknown. The study aimed to assess SPD's impact on iron overload-induced bone loss in elderly rats. In our aged rat model, we found that iron overload negatively influences bone metabolism and remodeling, resulting in decreased bone mineral density and increased bone loss. However, SPD treatment effectively alleviated these harmful effects, as shown by reduced serum levels of MDA and increased SOD and GSH levels. Additionally, SPD-treated rats exhibited enhanced bone mass and higher expression of OC, BMP2, SIRT1, and SOD2 in their bones. Moreover, SPD restored the imbalance in bone metabolism by counteracting the inhibition of osteogenic differentiation and promoting osteoclast differentiation induced by iron overload in MC3T3-E1 and RAW264.7 cells affected by EX527. In summary, our findings suggest that SPD's antioxidant properties may exert anti-osteoporosis effects through activation of the SIRT1/SOD2 signaling pathway.

KEYWORDS

Iron overload; oxidative stress; spermidine; bone mass; bone metabolism; senile osteoporosis; SIRT1/SOD2 signaling pathway; MC3T3-E1; RAW264.7

1. Introduction

Osteoporosis, which is characterized by a decrease in bone density and the deterioration of bone tissue, is a common health issue among the elderly population [1]. As people age, their bodies produce less new bone tissue, and the bones become thinner and weaker, increasing the risk of osteoporosis [2,3]. Osteoporosis is often referred to as a 'silent disease' because it progresses slowly and may not cause any symptoms until it reaches an advanced stage [4,5]. There are several factors that can increase the risk of developing osteoporosis, including a family history of the disease, a sedentary lifestyle, a diet low in calcium and vitamin D, and certain medications [6]. Additionally, older adults who smoke or drink alcohol regularly may be at a higher risk of developing osteoporosis [7]. To prevent osteoporosis, it is important for elderly individuals to maintain a healthy lifestyle that includes regular exercise, a balanced diet rich in calcium and vitamin D, and quitting smoking and excessive alcohol consumption [6]. Therefore, early identification and removal of risk factors can help elderly individuals maintain their independence and quality of life.

Iron participates in numerous biological processes in the body, playing an important role in many processes such as oxygen transport, DNA synthesis and muscle metabolism [8]. Iron levels in pathological concentrations including iron overload and iron deficiency contribute to various human pathologies such as cancer and anemia [9]. Iron overload contributes to developing many blood disorders such as aplastic anemia, hereditary hemochromatosis, thalassemia and sickle cell disease [10]. In addition, recent studies have confirmed that physiological iron concentrations is required to maintain bone reconstruction and bone health [11,12]. Moreover, excessive accumulation of iron can result in the generation of a significant amount of reactive oxygen species (ROS) via the fenton reaction [13,14]. This process has the potential to induce detrimental effects on osteoblast DNA, protein, mitochondria, and other cellular components [13,14]. Consequently, it disrupts the normal equilibrium within bone tissue and ultimately leads to a decline in bone mass and impaired healing capacity [13,14].

Spermidine (SPD) is a naturally occurring organic compound that belongs to the family of polyamines, which are essential bioactive molecule in the human body [15]. SPD plays an important role in various physiological processes, including cell growth and proliferation, DNA synthesis, and the regulation of ion channel activity [16]. In recent years, there has been increasing interest in the potential health benefits of SPD [17]. By increasing glutathione levels, SPD can effectively reduce oxidative stress and thereby reduce the risk of many diseases associated with chronic inflammation and oxidative damage [18]. Studies have shown that SPD can positively impact bone health by promoting the growth and differentiation of osteoblasts, the cells responsible for bone formation [19]. Additionally, studies have reported that mice fed a diet supplemented with SPD had higher bone mineral density and better bone quality compared to mice not receiving the supplement [20].

Based on the aforementioned information, it is reasonable to postulate that SPD may confer protection against the deleterious effects of iron overload on bone health. However, it remains unclear whether SPD can effectively mitigate the

CONTACT Wanshu Zhou 1474888701@qq.com Department of Gerontology, The Second Affiliated Hospital of Wannan Medical College, No.10Kangfu Road, Jinghu District, Wuhu City, Anhui 241000, People's Republic of China; Zhou-Shan Tao tzs19900327@126.com Department of Orthopedics, The First Affiliated Hospital of Wannan Medical College, Yijishan Hospital, No. 2, Zhe Shan Xi Road, Wuhu, Anhui 241001, People's Republic of China

negative impact of iron overload on bone density by reducing oxidative stress. This is because SPD actively participates in the antioxidant system and safeguards osteoblasts from oxidative damage. Hence, our current study aims to investigate the potential benefits of SPD in preventing bone loss caused by iron overload using a rat model of senile osteoporosis. Additionally, we aim to explore the underlying mechanisms involved in this process.

2. Materials and methods

2.1. Experimental animals and treatment

The study involved male Sprague–Dawley (SD) rats, aged 24 months and weighing between 500–550 g. These rats were housed in stainless steel cages under sterile conditions, with access to tap water and standard rodent chow. The environment maintained a constant temperature of 23 °C and followed a 12-hour light–dark cycle. Then, the animals were randomly divided into four groups of 10 rats each: Con group, FAC group, FAC+LSPD group, and FAC+HSPD group. The elderly rats in the FAC+LSPD group and FAC +HSPD group were administered intraperitoneal injections of ferric ammonium citrate (Sigma-Aldrich) three times a week, with a dosage of 40 mg/kg. Additionally, they received spermidine (Sigma-Aldrich) at either 10 mg/kg/day or 20 mg/kg/day for a duration of 12 weeks. These dosages have been previously utilized in another studies [21–23]. The Sham group and OVX group rats received daily subcutaneous injections of a saline solution. Each group of rats was administered calcine green (25 mg/kg) 13 and 3 days prior to sacrifice. At the end of the experiment, the rats were humanely euthanized, and blood samples as well as bilateral femurs were collected for subsequent analysis. The experimental protocols received formal approval from Wannan Medical College's Institutional Animal Care Committee (WNMC-AWE-2024203; March 6, 2024) and strictly adhered to globally recognized animal welfare protocols throughout implementation.

2.2. Micro-CT evaluation

The evaluation of trabecular bone density and microscopic parameters in the distal femur was conducted using micro-CT (micro-CT 100, Scanco Medical AG, Bassersdorf, Switzerland), following the methodology described in previous studies [24,25]. The sample was subjected to Micro-CT scanning with a resolution of 15 μm, using parameters of 70 kV and 200 μA. The integration time was set at 300 ms, and the resulting data was reconstructed with an isotropic voxel size of 5 mm. In order to analyze changes in bone trabecular structure, a volume of interest (VOI) was selected starting from below the growth plate and extending for a distance of 2 mm with a width of 250 mm. Within this VOI zone, various bone morphometric parameters such as bone volume per total volume (BV/TV), bone trabecular thickness (Tb.Th), trabecular number (Tb.N), trabecular spacing (Tb.Sp), Bone mineral Content (BMC) and Bone mineral density (BMD) were calculated.

2.3. Histological evaluation

Bone specimens were fixed in 10% formalin overnight, washed, decalcified in 10% EDTA (pH 7.4) at 4 °C for 28 days before paraffin-embedding. The horizontally oriented femur sections with 4-micrometer-thick were collected for HE, Masson and immunohistochemical staining with SIRT1 and SOD2. The HE and Masson staining procedures are strictly followed as per the provided instructions, and images are captured using an optical microscope. For immunofluorescence staining, bone sections were subjected to incubation with primary antibodies targeting Bone morphogenetic protein-2 (BMP2, Abcam, 1:100), osteocalcin(OC, Abcam, 1:100), SIRT1 (Abcam, 1:100) and SOD2 (Abcam, 1:100) at a temperature of 4°C. Following this step, the secondary antibodies conjugated with fluorescence (Jackson Immuno Research), diluted at a ratio of 1:250 as per the manufacturer's instructions, were incubated at room temperature for a duration of 1 h. DAPI staining (Thermo Fisher Scientific) was employed to visualize the cell nuclei. The acquired images were subsequently analyzed using image J software and a confocal microscope (Carl Zeiss Axiovert, Germany).

Samples that were not decalcified went through dehydration with a succession of alcohol concentrations before being embedded in PMMA embedding agent and cut into 50 μm sections using a diamond tissue microtome (SAT-001-E300CP; EXAKT, Hamburg, Germany). Fluorescence microscopy was then employed to monitor the bone mineralization process.

2.4. Assessment of bone metabolism and oxidative stress

The ELISA kits for assessing serum bone metabolism markers, including CTX-I, PINP, and TRAP, were procured from Beijing Fangcheng Biotechnology Company in Beijing, China. Nanjing Jiancheng Bioengineering Institute in Nanjing, China provided commercial kits to examine oxidative stress-related indicators like SOD, MDA, and GSH as per the manufacturer's guidelines.

2.5. Culture of MC3T3-E1 cells and RAW264.7 cells

The MC3T3-E1 cells, derived from mice preosteoblasts, were acquired from the Chinese Academy of Sciences in Shanghai, China. They were cultured using Dulbecco's modified Eagle's medium (DMEM, Gibco) supplemented with 10% fetal bovine serum (FBS), and 1% penicillin–streptomycin combination, following previously established protocols [25–27]. RAW264.7 cells obtained from a Chinese company (Shanghai Bangjing Industrial Co., Ltd.) were utilized to investigate the impact of various intervention conditions on the differentiation of osteoclasts. The RAW264.7 cells were cultured in DMEM supplemented with 10% fetal bovine serum (Gibco) at a temperature of 37°C in an incubator that maintained a CO_2 concentration of 5%. To induce osteoclast differentiation, the DMEM medium was supplemented with 1% penicillin streptomycin (Solarbio, Beijing, China) and RANKL at a concentration of 50 ng/mL. MC3T3-E1 and RAW264.7 cells were utilized in all experiments, with a seeding density of 1×10^4 cells/ml on the specimens. The cells were then randomly assigned to incubate with the following factors: (1) Control group (Con); (2) treatment group with ammonium ferric citrate (FAC, sigma) at a concentration of 10 mM from Sigma (FAC); (3) FAC+SPD treatment group using FAC and SPD; (4) FAC+SPD/EX527 treatment group where EX527, a SIRT1 inhibitor at a concentration of 10 μM from Selleck Chemicals, Houston, TX, USA was added to FAC+SPD mixture. The dosages for EX527 and FAC were

Table 1. The primers used in this study.

Gene	Accession number in Gene Bank	Forward Primer sequence (5′-3′)	Reverse Primer sequence (5′-3′)
SIRT1	NC_000076.7	GCGGGAATCCAAAGGATAAT	CTGTTGCAAAGGAACCATGA
CAT	NC_058377.1	TGGGATCTCGTTGGAAATAACAC	TCAGGACGTAGGCTCCAGAAG
SOD2	NC_000006.12	GGGGATTGATGTGTGGGAGCACG	AGACAGGACGTTATCTTGCTGGGA
SOD1	NT_037436.4	GGTGGGCCAAAGGATGAAGAG	CCACAAGCCAAACGACTTCC
GAPDH	NC_000012.12	AGAAAAACCTGCCAAATATGATGA	CTGGGTGTCGCTGTTGAAGTC

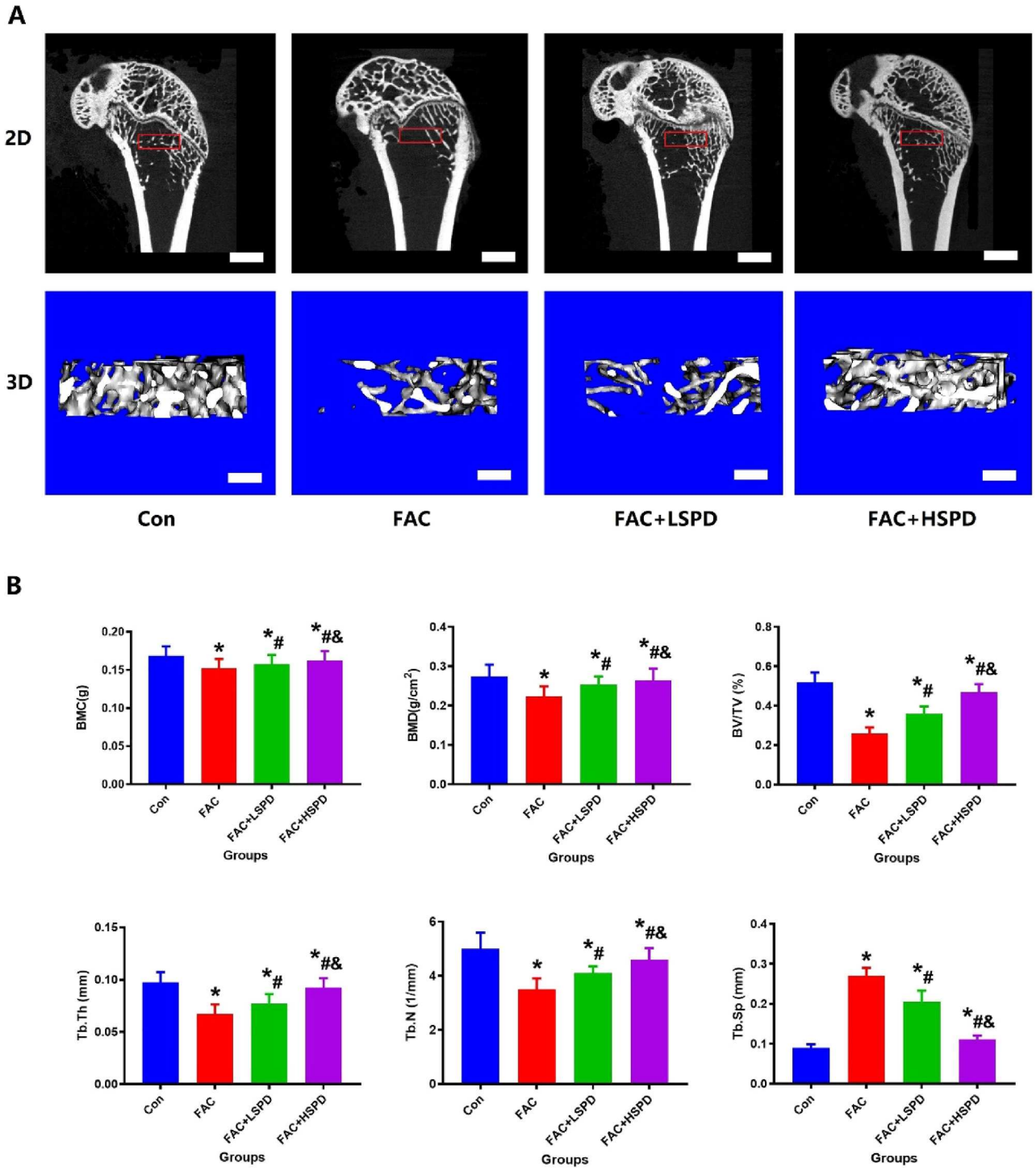

Figure 1. SPD has the potential to mitigate the negative impact of FAC on bone mass in elderly rats. A. Depicting alterations in the microstructure of distal femoral trabecular bone, this study presents representative 2D and 3D micro-CT images from the Con, FAC, FAC+LSPD, and FAC+HSPD groups (n = 5). The scale bar represents 2 mm. B. Quantitative outcomes of trabecular bone in the metaphysis of the femur, encompassing parameters such as bone mineral content (BMC), connectivity density (Conn.D), ratio of bone volume to total volume (BV/TV), trabecular number (Tb. N), trabecular thickness (Tb. Th), and trabecular spacing (Tb.Sp) (n = 5).

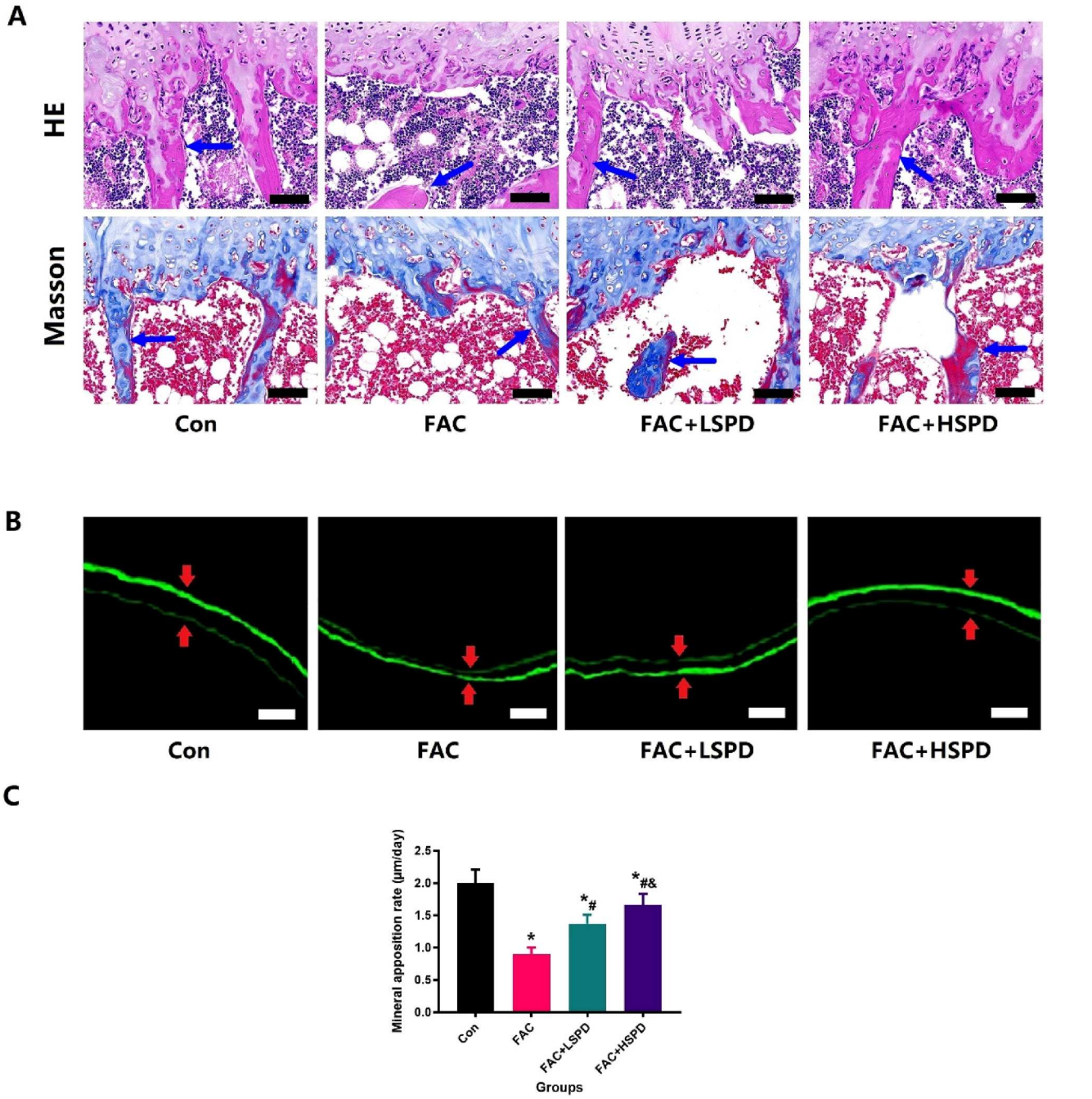

Figure 2. The potential of SPD to increase bone trabecular mass bone mineralization rate(BMR) in FAC treated rats from Con, FAC, FAC+LSPD, and FAC+HSPD groups. A. Representative HE and Masson staining observed changes in trabecular bone structure and medullary cavity cells in the distal femur (X40), blue arrow represents the trabecular bone. B. Representative fluorescence labeled images of changes in cortical BMR of femoral bone in each group of rats (X200) (n = 5), the red arrows represent the distance of bone mineralization; C. Quantitative detection of cortical BMR of fluorescently labeled femoral bone (n = 5).

selected based on previous studies [21,22]. Subsequently, the culture medium was replaced every 48 h until the end of the cell experiment.

2.6. Cell count kit-8 (CCK-8) assay

Osteoblast proliferation was assessed using CCK-8 at 24, 48 and 72 h of incubation as our previously described [28,29]. The measurement of cell viability was conducted using a microplate reader (BioTek, EPOCH, USA) with detection at a wavelength of 450 nm.

2.7. Alkaline phosphatase staining (ALP) and alizarin red staining (RES)

To assess the differentiation and mineralization ability of osteoblasts, we utilized the BCIP/NBT alkaline phosphatase chromogenic kit (Beyotime, Shanghai, China) and alizarin red staining solution kit (Solarbio, Beijing, China), following the recommended protocol. After 7 and 21 days of incubation, we evaluated the osteoblast differentiation and mineralization ability of MC3T3-E1 cells using ALP staining and RES staining as previously described [28,29]. The intensity of ALP expression and calcified nodules were quantitatively analyzed using Image J software (National Institutes of Health, Bethesda, Maryland, USA).

2.8. Evaluation of oxidative stress

The assessment of oxidative stress was conducted using 2′,7′-dichlorofluorescein diacetate (DCFH-DA, Sigma, St. Louis, MO) and Mito SOX™ Red mitochondrial superoxide indicator (Mito SOX™, Sigma, St. Louis, MO). Following a 48-hour

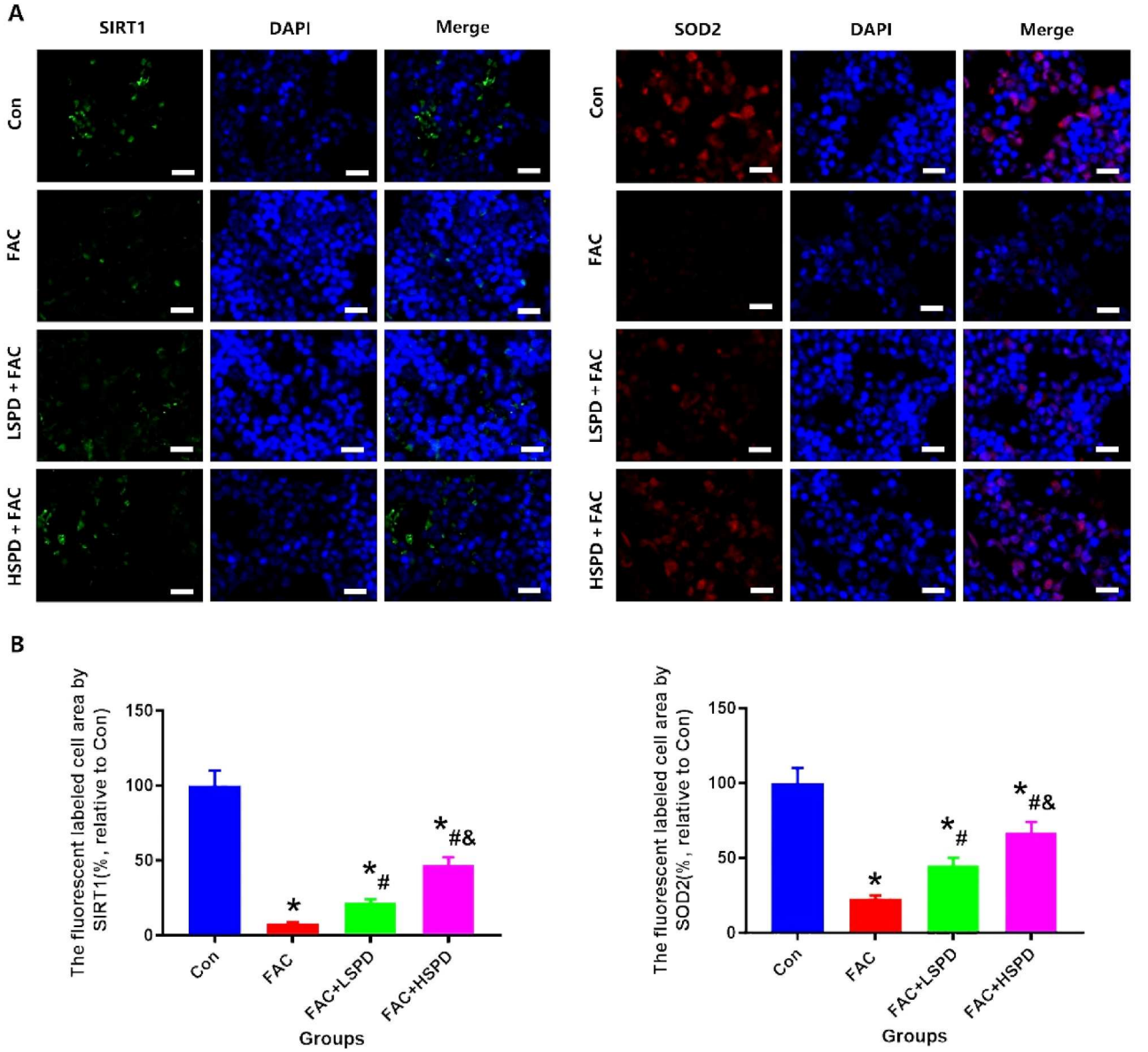

Figure 3. Immunohistochemical analysis revealed that the administration of SPD systemically had the potential to modify SIRT1 and SOD2 expression in bone tissue located in the femoral metaphysis of aged rats with iron overload. A. Representative SIRT1 and SOD2 staining images in bone tissue from Con, FAC, FAC +LSPD, and FAC+HSPD groups. Scale bar: 25 μm (n = 5). B. The fluorescence-labeled bone tissue in the femoral metaphysis served as a representation of the quantitative outcomes obtained from SIRT1 and SOD2 analysis (n = 5).

intervention period, the cells were exposed to 10 μmol/L DCFH-DA for 30 min at a temperature of 37 °C to observe the fluorescence intensity of DCF. Simultaneously, the cells were treated with a light-protected solution containing 5 μM MitoSOX for 10 min at a temperature of 37 °C as per the manufacturer's instructions. The stained cells were then observed under a fluorescence microscope along with counterstains. The levels of Malondialdehyde (MDA) and total SOD activity in the cells were quantified using a malondialdehyde Detection Assay kit (APPLYGEN) and Superoxide Dismutase Activity Assay Kit (Abcam), respectively.

2.9. Cellular immunofluorescence

After a 48-hour period of various interventions, osteoblasts were fixed using a solution containing 4% paraformaldehyde (PFA) and permeabilized with 0.5% X-100 Triton (Sigma-Aldrich, USA) in PBS for a duration of 10 min. Following this, non-specific binding of antibodies was prevented by blocking with a mixture consisting of 10% Goat Serum and 0.2% Tween-20 in HBSS (Sigma-Aldrich, USA), which was carried out at room temperature for one hour. Subsequently, the treated cells were exposed to primary antibodies (SIRT1:ab189494; SOD2:ab208156; dilution ratio of 1:500; abcam, USA) overnight at a temperature of 4°C. Cells that underwent treatment with these primary antibodies were then subjected to incubation with secondary antibody (Alexa Fluor 594-conjugated goat anti-rabbit IgG; dilution ratio of 1:1000; Abcam) for a duration of sixty minutes under dark conditions. DAPI staining solution from Thermo Fisher Scientific was utilized to stain the cell nuclei. The acquired images were analyzed using image J software and captured using a confocal microscope manufactured by Carl Zeiss Axiovert in Germany.

2.10. Measurement of mitochondrial membrane potential

To verify alterations in the potential of mitochondrial membrane, we employed a combination of tetramethylrhodamine

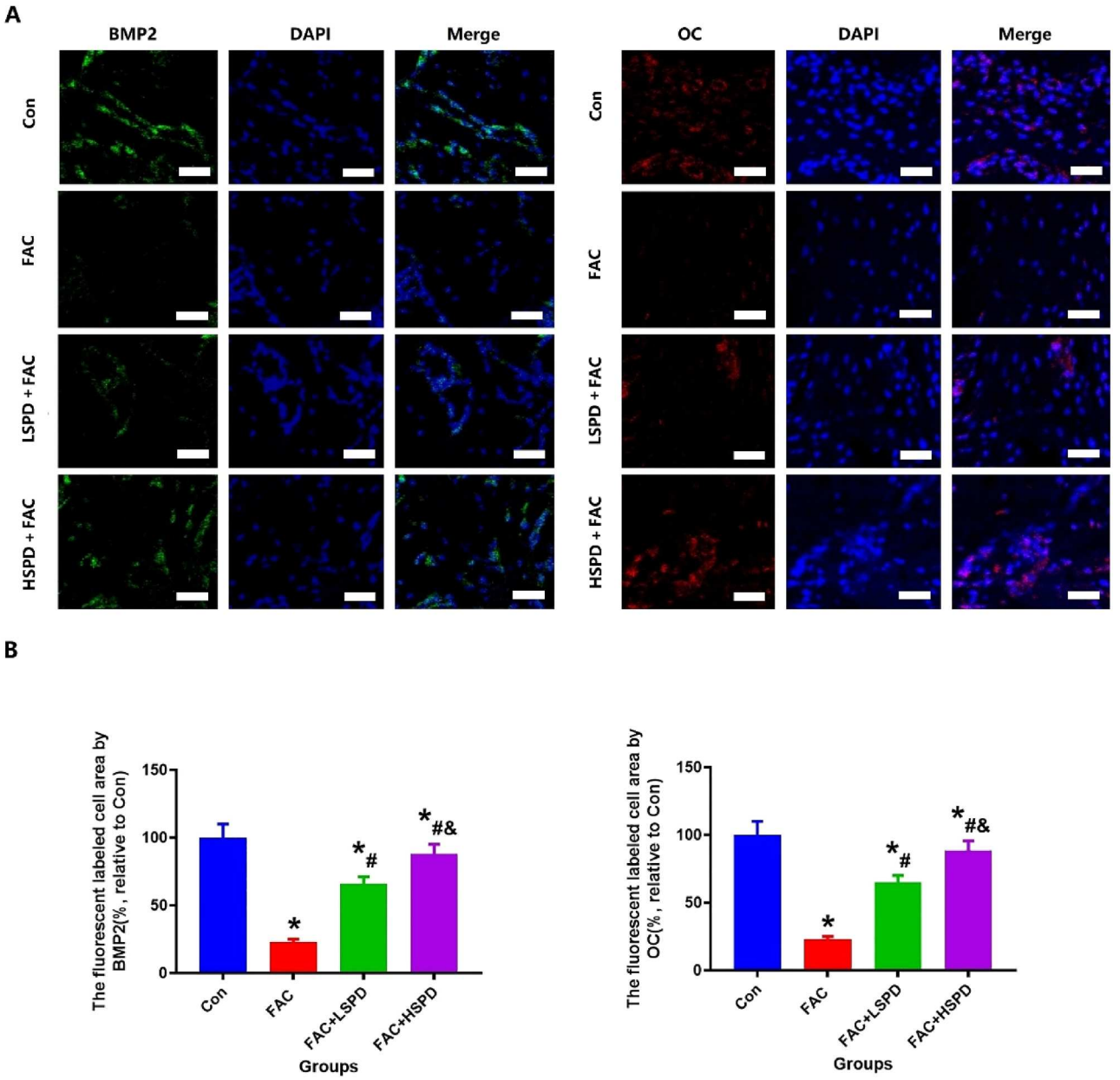

Figure 4. Immunohistochemical analysis revealed that the administration of SPD systemically had the potential to modify BMP2 and OC expression in bone tissue located in the femoral metaphysis of aged rats with iron overload. A. Representative BMP2 and OC staining images in bone tissue from Con, FAC, FAC+LSPD, and FAC+HSPD groups. Scale bar: 25 μm (n = 5). B. The fluorescence-labeled bone tissue in the femoral metaphysis served as a representation of the quantitative outcomes obtained from BMP2 and OC analysis (n = 5).

methyl ester (TMRM, 100 nM, Life Technologies) and Mitotracker Green (Mitogreen, 100 nM, Life Technologies) for simultaneous staining. This allowed us to observe and assess the condition of oxidative stress within the treated cells. After 48 h of intervention, TMRM and Mitogreen staining were performed as previously described [30]. The results of TMRM(excitation wavelengths = 543 nm) and Mitogreen(excitation wavelengths = 488 nm) were captured using Laser confocal microscope. The quantification of mitochondrial membrane potential was determined using Image J software.

2.11. RNA extraction and real-time PCR

The TRIzol reagent (Invitrogen) was used to extract total RNA from osteoblasts following various therapeutic interventions. For cDNA preparation, a commercial PrimeScript reverse transcription kit (TaKaRa, Tokyo, Japan) was employed. Real-time PCR amplification reactions were conducted using the SYBR Green PCR Kit (TaKaRa). The relative expression of the target gene was determined by normalizing Ct values with glyceraldehyde-3-phosphate dehydrogenase (GAPDH) levels. Please refer to Table 1 for the primer sets utilized in this study.

2.12. Statistical analysis

The experimental results were expressed as mean ± standard deviation with n = 5/group. The statistical software SPSS (19.0) was employed to analyze the experimental data. All data were assessed for normality to ensure compliance with the assumptions of parametric testing. Subsequently, One-way analysis of variance (ANOVA) was conducted to perform multiple between-group comparisons, followed by Tukey's post hoc test. A value of P?0.05 was considered to reflect significance. *Vs. Con group, $P<0.05$; #Vs. FAC, $P<0.05$; &Vs. FAC +LSPD, $P<0.05$.

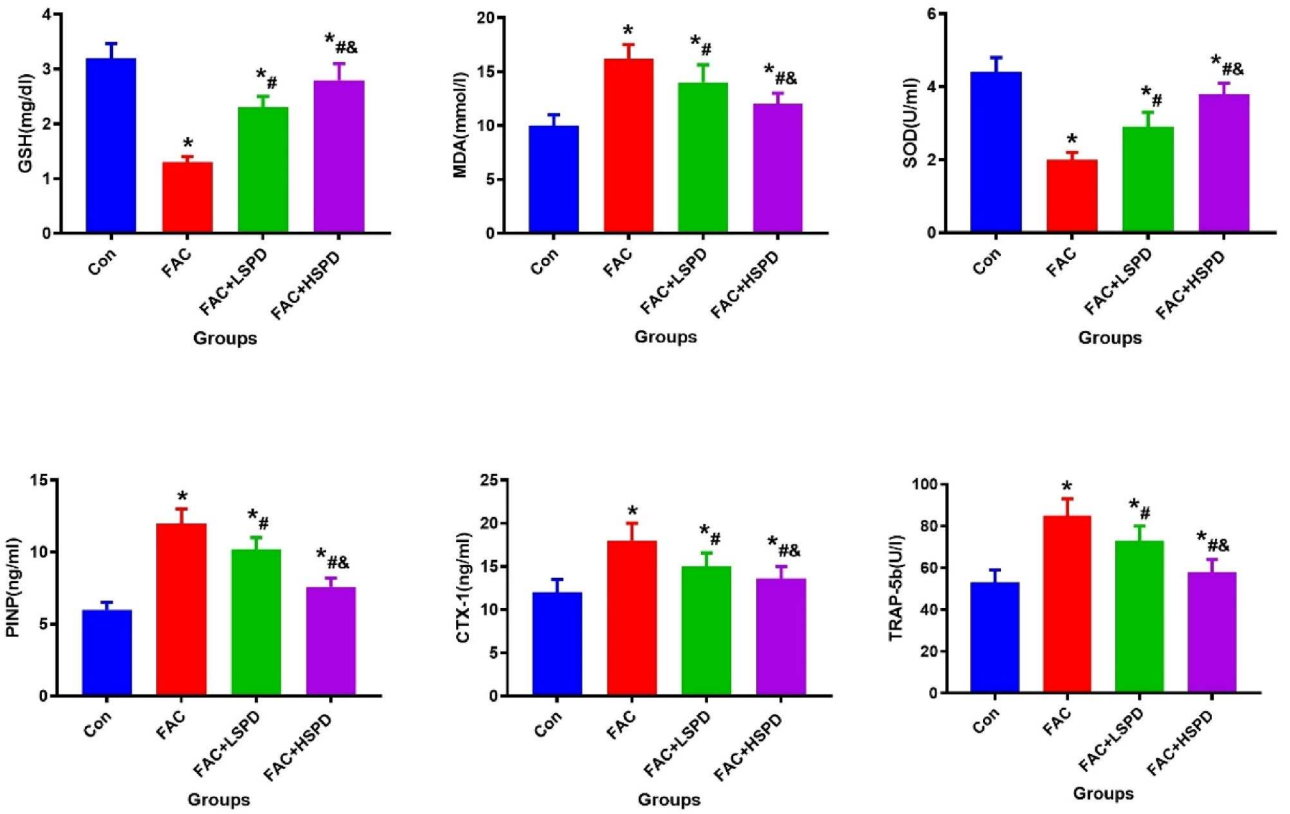

Figure 5. Systemic administration of SPD exhibits notable efficacy in reducing oxidative stress markers and effectively restoring the imbalanced bone metabolism equilibrium in aged rats with iron overload (n = 5).

3. Results

3.1. SPD treatment can improve bone mass and BMD in aged rats with FAC intervention

To assess the protective effects of SPD treatment against FAC-induced reduction in bone mass, we conducted imaging and histological examinations in an experimental model of senile rats. We utilized Micro-CT scanning and 3D reconstruction to observe the distal femoral trabecular bone in rats subjected to FAC treatment. Our findings revealed that the FAC treatment group exhibited significant bone sparsity, which was noticeably mitigated with SPD treatment, especially in the HSPD treatment group (Figure 1). Micro-CT analysis showed higher BV/TV, Tb. Th, Tb. N, and BMD, along with lower Tb. Sp in SPD-treated rats compared to the FAC group, revealing the adverse effects of excessive iron accumulation on skeletal well-being in elderly rats. Notably, SPD reversed this adverse effect based on animal experiments. Additionally, histopathological examination using HE and Masson staining confirmed our imaging findings, showing that bone mass loss in iron overload rats was associated with increased adipocyte production, a phenomenon which was reversed by SPD treatment (Figure 2A). Meanwhile, we also found that SPD could significantly increase bone mineralization rate in FAC treated rats (Figure 2 B,C).

3.2. SPD regulates SIRT1/SOD2 signaling and bone metabolism in experimental senile rats with FAC intervention.

Due to the influential role of the SIRT1/SOD2 signaling pathway in FAC-induced reduction in bone mass [21,22], we employed immunofluorescence techniques to label SIRT1 and SOD2 for bone reconstruction analysis (Figure 3 A). Our results demonstrated a significant reduction in the expression of SIRT1 and SOD2 following FAC treatment compared to the control group ($P<0.05$). Furthermore, SPD-treated rats exhibited significantly increased expression of SIRT1 and SOD2 compared to the FAC group ($P<0.05$, Figure 3 B). Meanwhile, we found that BMP2 and OC were highly expressed in SPD-treated rats ($P<0.05$, Figure 4).

Additionally, we assessed various particular markers related to bone metabolism and indicators of oxidative stress in serum within each group, including CTX-I, PINP, TRAP, MDA, GSH and SOD. Our results demonstrated that FAC treatment significantly reduced GSH and SOD levels while increasing CTX-I, PINP, TRAP, and MDA levels compared to the Con group ($P<0.05$, Figure 5). Conversely, SPD-treated rats exhibited significantly increased GSH and SOD levels, along with reduced CTX-I, PINP, TRAP, and MDA levels compared to the FAC group ($P<0.05$, Figure 5). These results indicate that the presence of excessive iron significantly impacts bone metabolism and oxidative stress in elderly rats. Moreover, treatment with SPD demonstrates a notable ability to decrease elevated levels of bone turnover and oxidative stress.

3.3. SPD improves the proliferation and of MC3T3-E1 cells

In order to detect the effect of different concentrations of FAC and SPD on cell proliferation rate, different concentrations of SPD (1, 100, 500, 1000 μM) were applied to cells for 24 h in this experiment, and the cell proliferation rate was detected by CCK-8 assay. As shown in Figure 6A, the cell proliferation rate shows a downward trend when the SPD concentration ranges from 1 μM to 100 μM ($P< 0.05$). The subsequent cell

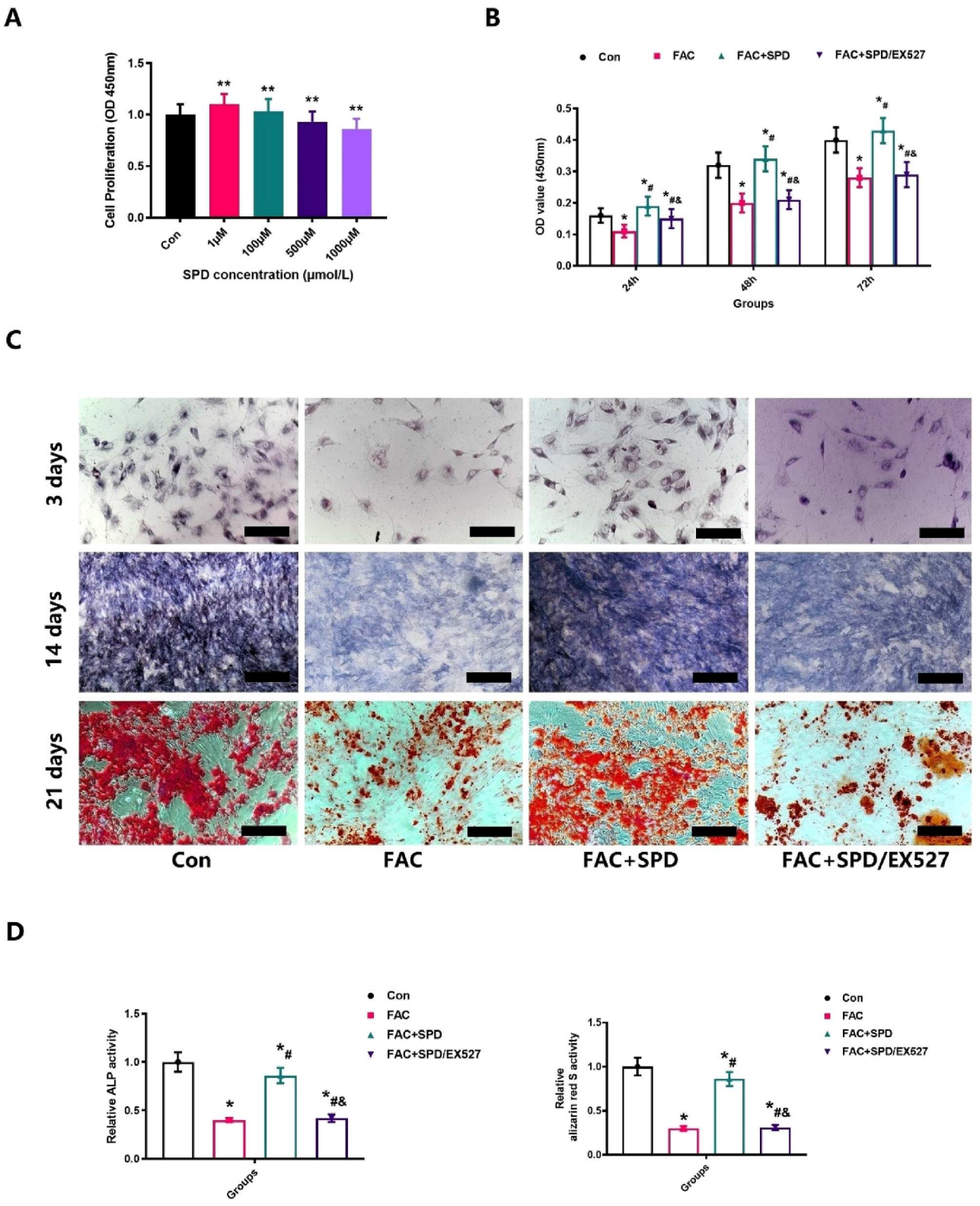

Figure 6. Effect of SPD on the proliferation rate and osteogenic differentiation of MC3T3-E1 cells with FAC treatment. A. The effect of SPD on cell proliferation rate at different concentrations (1, 100, 500, 1000 μM) was detected by CCK-8 for 24 h (n = 5); B. The effect of SPD and FAC on the rate of cell proliferation was detected by CCK-8 at a concentration of 1 μM (n = 5). C. After adding SPD, the expression of alkaline phosphatase and formation of calcified nodules increased significantly (n = 5). D. For the quantitative analysis of alkaline phosphatase staining and alizarin red staining positive areas (n = 5).

experiments employed a dosage of 1 μm for SPD. When the concentration of SPD was fixed at 1 μM, the effects of different action times (24 h, 48 h, 72 h) on the proliferation rate of MC3T3-E1 were investigated. As shown in Figure 6 B, CCK-8 results showed that the cell proliferation rate of FAC was reduced at 24 h, 48 h, 72 h after FAC treatment, while SPD treatment demonstrated a notable ability to mitigate the detrimental impacts caused by FAC, and it was observed that EX527 could potentially interfere with the aforementioned effects induced by FAC ($P< 0.05$).

3.4. SPD protects MC3T3-E1 against the effects of FAC damage on osteogenesis.

Based on the findings from ALP staining and alizarin staining (Figure 6 C), the treatment of FAC resulted in a

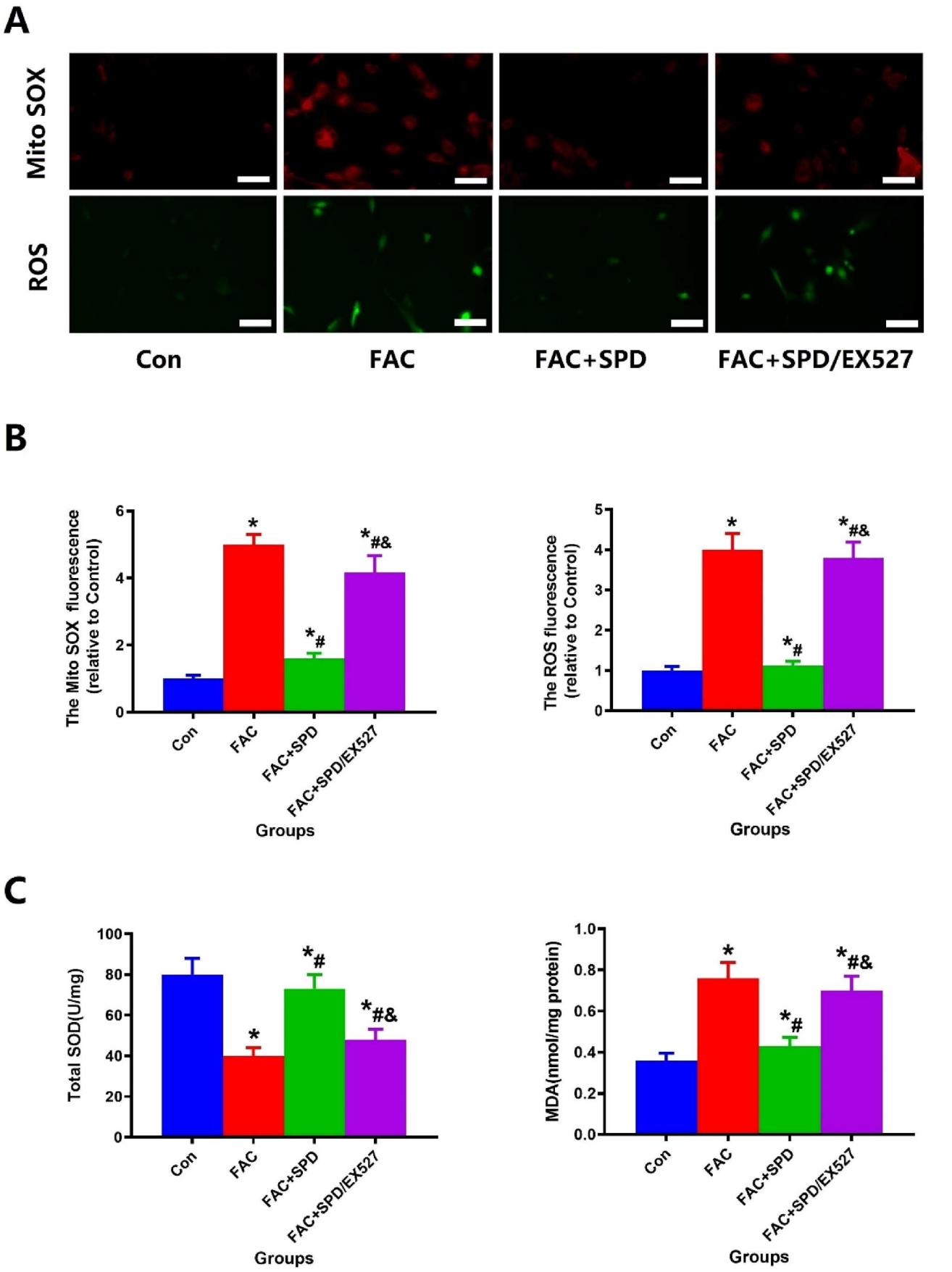

Figure 7. Assessment of the impact of SPD intervention on ROS and Mito SOX production in MC3T3-E1 cells treated with FAC. A. After the implementation of SPD, there was a noticeable reduction in the quantities of ROS and Mito SOX generated in MC3T3-E1 cells subjected to FAC treatment (n = 5). B. Quantitative analysis of ROS and Mito SOX via immunofluorescence staining (n = 5). C. Changes in the levels of SOD and MDA were noted after the application of SPD and FAC interventions (n = 5).

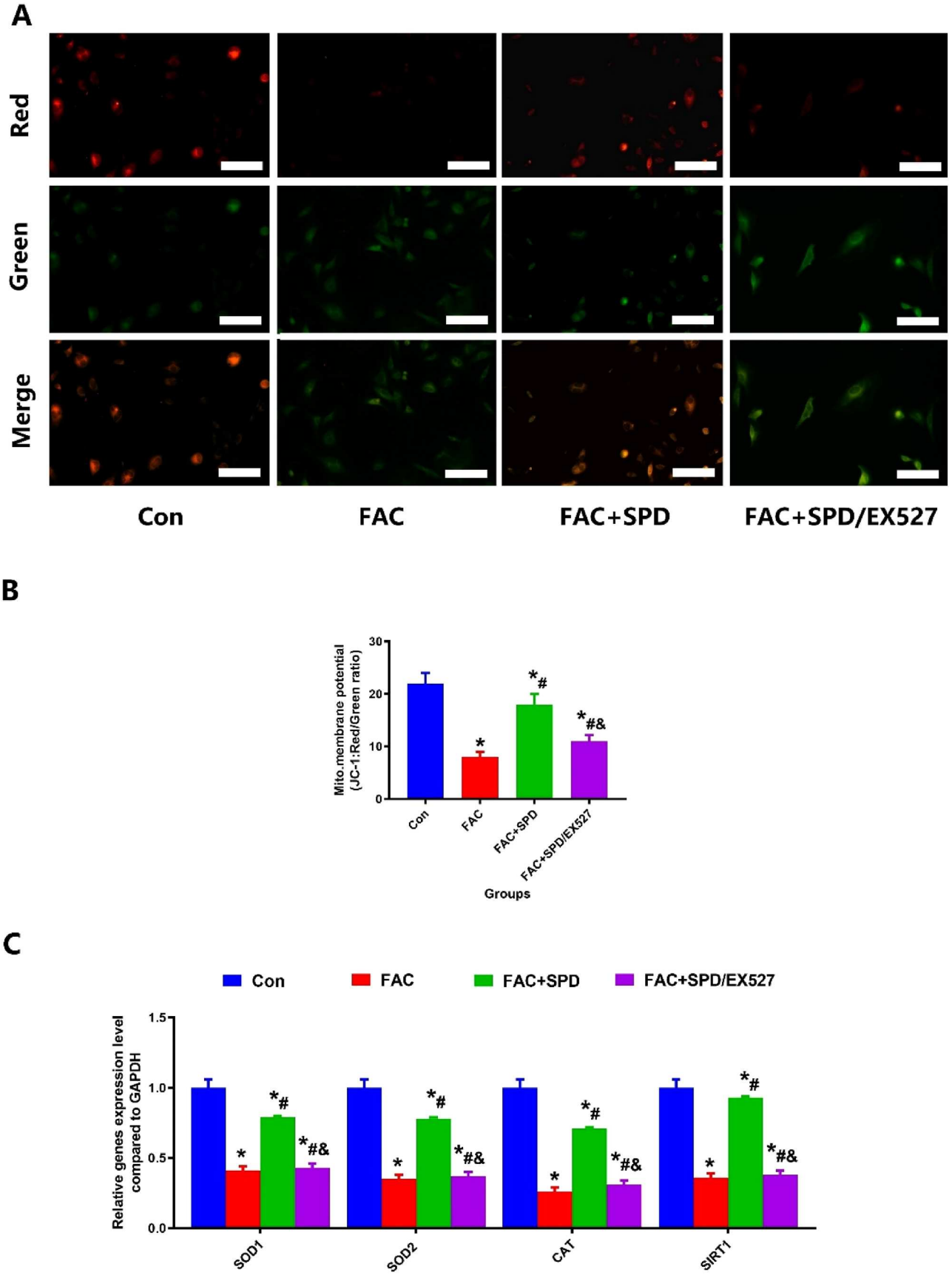

Figure 8. SPD therapy promotes recovery of mitochondrial membrane potential activity in the presence of iron overload by JC-1 staining. A. JC-1 staining was observed at high magnification to assess the ability of SPD to significantly improve the recovery of mitochondrial membrane potential in iron overload MC3TE-E1 (Scale bar = 25 μm) (n = 5); B. Quantitative analysis of changes in mitochondrial membrane potential in MC3TE-E1 with iron overload after SPD intervention (n = 5). C. RT-PCR were assess the ability of SPD to significantly improve the related genes expression in iron overload MC3TE-E1 (n = 5).

significant reduction in MC3T3-E1 cells' mineralization, calcium nodule formation, and overall activity. However, when treated with SPD, these adverse effects of FAC were significantly inhibited. Additionally, it was observed that EX527 interfered with the aforementioned effects of FAC (P<0.05, Figure 6 D).

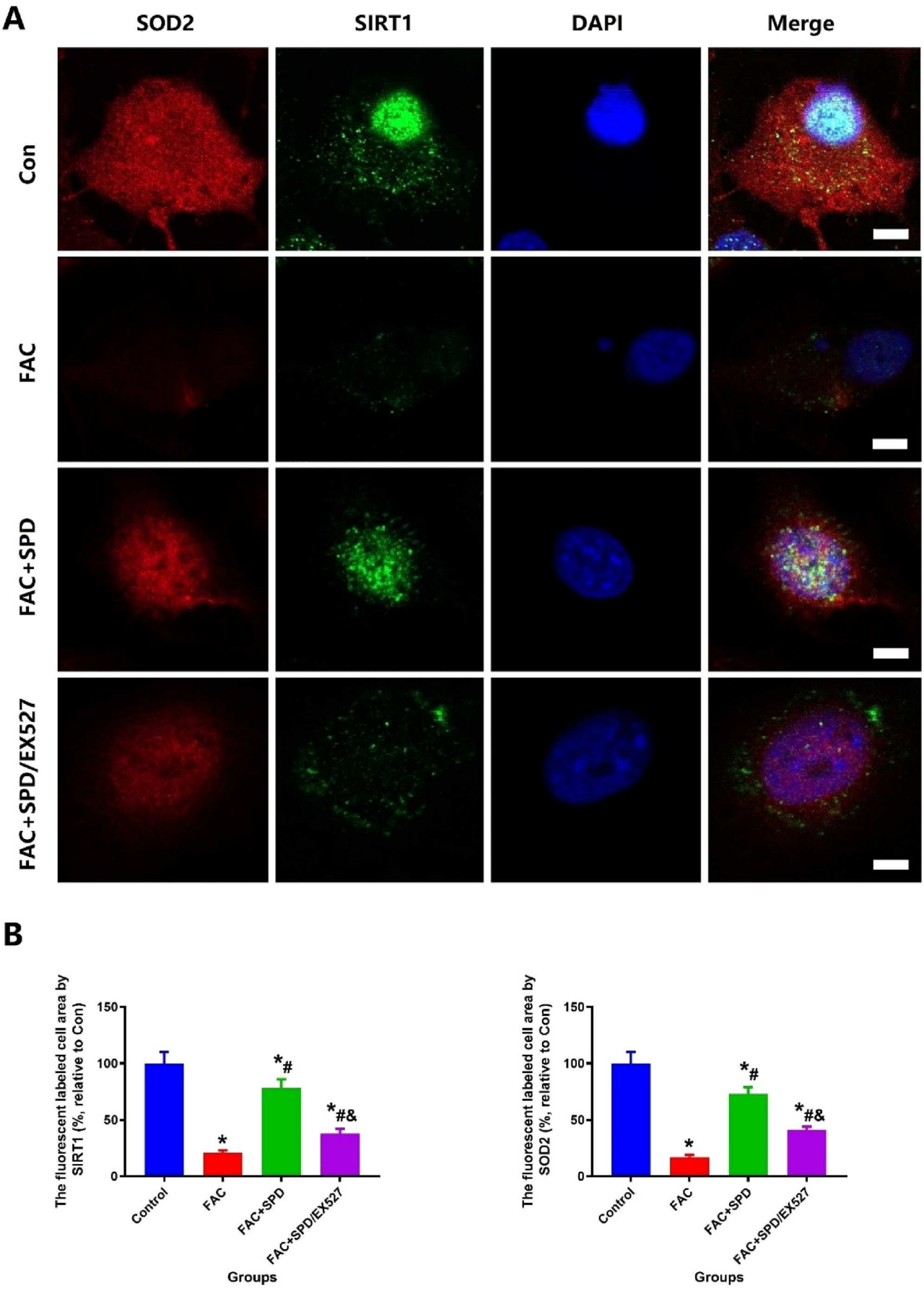

Figure 9. SPD therapy promotes SIRT1 and SOD2 expression in the presence of iron overload. A. immunofluorescence stainings were observed at high magnification to assess the levels of SIRT1 and SOD2 in MC3T3-E1 cells under conditions of iron overload (Scale bar = 25 μm) (n = 5); B. Quantitative analysis of changes in SIRT1 and SOD2 expression in MC3T3-E1 with iron overload after SPD intervention (n = 5).

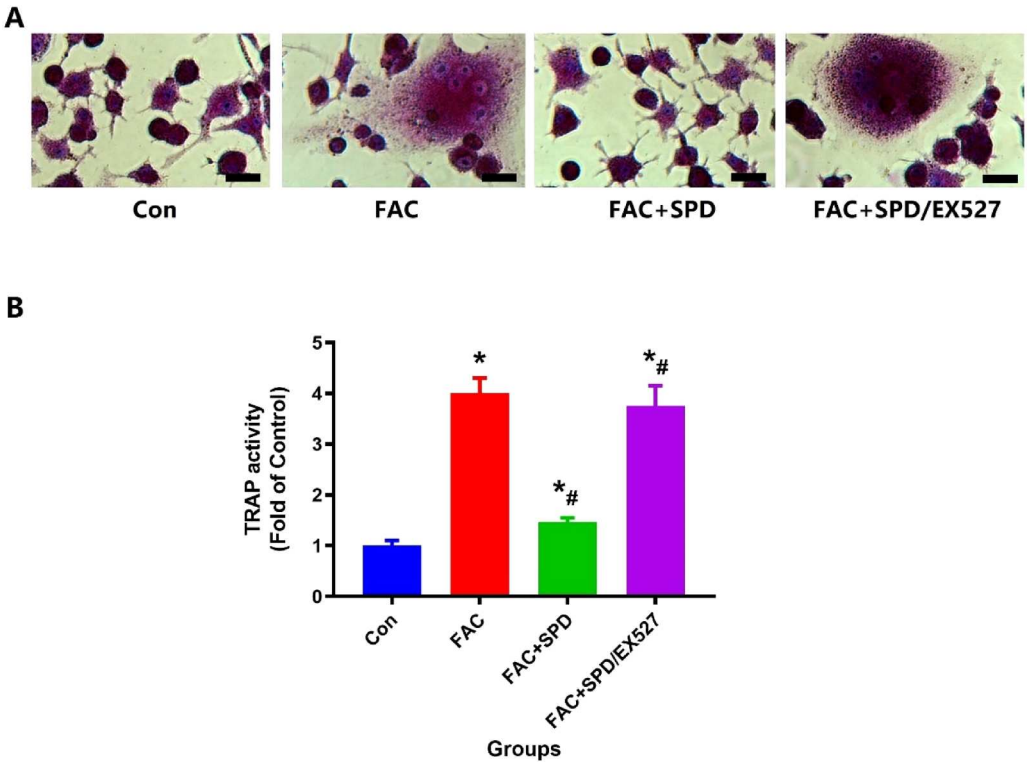

Figure 10. The osteoclast capacity in RAW264.7 cells, which was enhanced due to iron overload, experienced disruption upon treatment with SPD. A. SPD treatment significantly decreased the higher expression of TRAP caused by FAC (Scale bar = 50 μm) (n = 5). B. For the assessment of TRAP staining positive regions using quantitative analysis (n = 5).

Currently, numerous studies have provided evidence supporting the strong association between iron overload and oxidative stress-induced damage [21,22,31]. Therefore, we proceeded to investigate the oxidative stress status of MC3T3-E1 cells. We observed the presence of ROS and Mito SOX production in different groups of MC3T3-E1 cells following immunofluorescence staining (Figure 7 A). The findings clearly demonstrate a substantial increase in ROS and Mito SOX production after FAC treatment, while SPD administration effectively suppresses their production (P<0.05, Figure 7 B). Additionally, the levels of SOD and MDA in MC3T3-E1 cells also exhibited significant changes upon FAC and SPD interventions (P<0.05, Figure 7 C). We also assessed the impact of FAC on the mitochondrial membrane potential of MC3T3-E1 cells in each group using JC-1 detection and analysis, aiming to investigate cellular oxidative stress at the organelle level (Figure 7 A). The findings from JC-1 indicate that FAC induces damage to the mitochondrial membrane potential of MC3T3-E1 cells, while SPD exhibits a protective effect against this damage caused by FAC (P<0.05, Figure 8 B). The results of RT–PCR suggested FAC treatment significantly reduced SIRT1, SOD1, SOD2 and CAT expression compared to the Con group (P< 0.05, Figure 8 C). Conversely, SPD treated-MC3T3-E1 exhibited significantly increased SIRT1, SOD1, SOD2 and CAT expression compared to the FAC group (P < 0.05, Figure 8 C). Intriguingly, EX527 can effectively reverse all aforementioned alterations induced by FAC.

We conducted additional immunofluorescence staining using SIRT1 and SOD2 to directly investigate the signaling of SIRT1/SOD2. The findings indicated that FAC treatment led to a significant decrease in the expression of both SIRT1 and SOD2 compared to the control group (P< 0.05, Figure 9A). Conversely, MC3T3-E1 cells treated with SPD showed a notable increase in the expression of both SIRT1 and SOD2 compared to those treated with FAC (P < 0.05, Figure 9 B).

3.5. The inhibition of SPD on osteoclastic differentiation in FAC-treated RAW264.7 cells

According to the findings from TRAP staining (Figure 10 A) and quantitative analysis, it was observed that RAW264.7 cells exhibited a significant increase in TRAP expression following treatment with FAC (P < 0.05, Figure 10 B). However, the positive effects of FAC were effectively suppressed by SPD administration, while EX527 interfered with the aforementioned effects induced by FAC (P < 0.05, Figure 10 B).

4. Discussion

Patients who have excessive iron in their bodies are at a heightened risk of experiencing bone loss and fractures that result from weakened bones [11,12]. At present a large number researches have extensively demonstrated the antioxidant stress function and anti-aging efficacy of SPD [15]. The protective impact of this SPD on bone mass in individuals with iron overload remains uncertain. Through our animal experiments, we have observed that iron overload has a detrimental impact on bone mass and trabecular structure. Our in vitro experiments further revealed that iron overload induces oxidative stress and impairs osteoblast function, the cells responsible for bone formation. Moreover, treatment with SPD was found to ameliorate mitochondrial damage (the powerhouses of cells) caused by iron overload and reduce oxidative stress in osteoblasts. Consequently, SPD effectively improved compromised bone mass resulting from iron overload in aged rats. Furthermore, our findings suggest that SIRT1/SOD2 signaling inhibition due to iron overload plays

a pivotal role in mitochondrial damage and reactive oxygen species (ROS) generation within osteoblasts. On the other hand, the SIRT1/SOD2 signaling pathway is activated by SPD to provide protective effects on bones.

The current investigation utilized a model of senile osteoporosis to explore the detrimental impacts of excessive iron accumulation on bone mineral density (BMD), bone microstructure, and the potential protective effects of SPD against these adverse consequences in aged rats. For this experiment, we acquired male SD rats at 24 months old, which represents an advanced stage of aging. Additionally, previous research has indicated that older males may encounter similar levels of bone loss as observed in aging male SD rats [32,33]. Hence, our study opted for 24-month-old male SD rats as an appropriate animal model to replicate the skeletal metabolic status seen in elderly men undergoing age-related decline in bone mass. In this study, we observed a significant impact on bone remodeling due to FAC therapy, which resulted in accelerated bone mass loss and a substantial reduction in bone mineral density among elderly rats. To explore the protective effect of SPD and its underlying mechanisms, we developed an iron overload model in aged rats. However, there is limited understanding regarding the potential interaction between iron overload and SPD. Animal experiments have revealed that iron overload negatively affects bone health in aged rats by causing accelerated bone mass loss, degeneration of bone trabeculae, and disruption of bone metabolism. Fortunately, SPD has exhibited its capacity to protect bone health from the adverse consequences of excessive iron accumulation.

Considering the significant impact of osteoblast and osteoclast function on both bone formation and bone remodeling [34], we will conduct a comparison between MC3T3-E1 cells treated with SPD and/or FAC, and those left untreated. Our cellular investigations have unequivocally demonstrated that the incorporation of FAC into the culture milieu can significantly hinder both the proliferation and biological functions of MC3T3-E1 cells. However, upon administration of SPD to iron-overloaded MC3T3-E1 cells, we observed a remarkable attenuation of the deleterious effects induced by excessive iron exposure. RT–PCR analyses revealed a pronounced reduction in the transcription levels of osteoblast-related genes as well as those associated with oxidative stress markers, including SOD1, SOD2, CAT, and SIRT1 in MC3T3-E1 cells subjected to FAC when compared to their counterparts in the control group. Furthermore, subsequent cellular experiments demonstrated substantial reductions in JC-1 staining intensity and SOD enzymatic activity post-FAC intervention, while levels of ROS, Mito SOX, and MDA exhibited significant elevations. Changes in mitochondrial membrane potential and Mito SOX results are often associated with oxidative stress [35,36] as they reflect mitochondrial functional status. In our experiment, we observed a notable reduction in mineralization levels of MC3T3-E1 cells under iron overload conditions as evidenced by ALP staining and alizarin red assay. These revelations indicate that an overabundance of iron significantly compromises the functionality and mitochondrial efficacy of MC3T3-E1 cells, primarily due to heightened oxidative stress levels within osteoblasts. Moreover, treatment with SPD nearly fully reinstated cellular viability, operational capacity, and mitochondrial function when confronted with conditions of iron overload. Additionally, in vitro investigations utilizing RAW264.7 cells elucidated that the presence of FAC catalyzed the differentiation of osteoclasts, culminating in bone resorption and deleterious effects on osseointegration. Conversely, the process of osteoclastic differentiation triggered by FAC in RAW264.7 cells was notably impeded by SPD.

Multiple research studies have provided evidence for the crucial significance of the SIRT1 signaling pathway in safeguarding mitochondria against harm [37,38]. In order to further validate the impact of SIRT1, we employed the SIRT1 inhibitor EX527 to investigate the role of SIRT1 in SPD. Our observations revealed that EX527 counteracted the antioxidative stress effect of SPD. The intervention with FAC notably reduced both intracellular and bone tissue expression of SIRT1 and SOD2. These indicators, along with cell viability, were nearly restored following SPD treatment. However, EX527 was found to nullify the protective effect of SPD on cellular and mitochondrial activity as well as bone formation under iron-overloaded conditions. These experimental findings provide support for our in vivo study involving aged rats, which demonstrated impaired osteoblast activity, function, and bone formation due to iron overload. Moreover, it was observed that SPD can alleviate oxidative stress in vivo and within cells by activating the signaling pathway mediated by SIRT1. As a result, this prompts the revival of osteoblast function and activity, ultimately leading to an enhancement in bone mass.

Conclusions

In summary, our research findings validate that excessive iron levels impair the functioning of mitochondria and MC3T3-E1 cells, hinder bone formation, and stimulate bone resorption by increasing intracellular ROS levels. SPD enhances the performance and functionality of mitochondria and osteoblasts, inhibits the differentiation of osteoclasts, and promotes a reduction in intracellular ROS caused by iron overload in aged rat models through activation of the SIRT1 signaling pathway. However, in the cellular experiment, we found ourselves devoid of positive control groups such as hydrogen peroxide, Tiron, or PEGSOD. Concurrently, there exists a notable deficiency in comprehensive investigations surrounding the mechanisms at play, particularly regarding their impacts on iron metabolism and transport proteins. Consequently, it is imperative that further research be conducted to elucidate these facets.

Disclosure statement

No potential conflict of interest was reported by the author(s).

Funding

This study was supported by a grant from Health Research Project of Anhui Province (AHWJ2023A20550), Wuhu Science and Technology Project (2020cg43), Key Project of Wannan Medical College (WK2024ZZD29, 2020ZF20) and Wannan Medical College Youth Project (WK2023ZQNZ62).

Data availability statement

The data that support the findings of this study are available from the corresponding author, [ZS Tao], upon reasonable request.

ORCID

Zhou-Shan Tao http://orcid.org/0000-0001-6300-9289

References

[1] Lee EN, Choe SY, Choi EH, et al. Effects of parity and breast feeding duration on the risk of osteoporosis in postmenopausal Korean women: a systematic review and meta-analysis. J Menopausal Med. 2019 Aug;25(2):100–107. doi:10.6118/jmm.19197

[2] Park E, Kim J, Kim MC, et al. Anti-osteoporotic effects of kukoamine B isolated from lycii radicis cortex extract on osteoblast and osteoclast cells and ovariectomized osteoporosis model mice. Int J Mol Sci. 2019 Jun 6;20(11):1–14.

[3] Wasilewski GB, Vervloet MG, Schurgers LJ. The bone-vasculature axis: calcium supplementation and the role of vitamin K. Front Cardiovasc Med. 2019;6:6. doi:10.3389/fcvm.2019.00006

[4] Fan L, Li J, Yu Z, et al. The hypoxia-inducible factor pathway, prolyl hydroxylase domain protein inhibitors, and their roles in bone repair and regeneration. Biomed Res Int. 2014;2014:239356.

[5] Tao ZS, Qiang Z, Tu KK, et al. Treatment study of distal femur for parathyroid hormone (1–34) and beta-tricalcium phosphate on bone formation in critical size defects in rats. J Biomater Appl. 2015 Oct;30(4):484–491. doi:10.1177/0885328215592854

[6] Martiniakova M, Babikova M, Mondockova V, et al. The role of macronutrients, micronutrients and flavonoid polyphenols in the prevention and treatment of osteoporosis. Nutrients. 2022 Jan 25;14(3):1–17. doi:10.3390/nu14030523

[7] Zhang Q, Hu S, He Y, et al. Monotropein protects against inflammatory bone loss and suppresses osteoclast formation and bone resorption by inhibiting NFATc1 via NF-κB and Akt/GSK-3β pathway. Nutrients. 2022 Sep 24;14(19):1–19.

[8] Chen S, Zhang J, Jiang S, et al. Self-Assembled superparamagnetic iron oxide nanoclusters for universal cell labeling and MRI. Nanoscale Res Lett. 2016 Dec;11(1):263. doi:10.1186/s11671-016-1479-5

[9] Bogdan AR, Miyazawa M, Hashimoto K, et al. Regulators of iron homeostasis: new players in metabolism, cell death, and disease. Trends Biochem Sci. 2016 Mar;41(3):274–286. doi:10.1016/j.tibs.2015.11.012

[10] Tanaka H, Espinoza J, Fujiwara R, et al. Excessive reactive iron impairs hematopoiesis by affecting both immature hematopoietic cells and stromal cells. Cells. 2019;8(3):1–16. doi:10.3390/cells8030226

[11] Nemeth E, Ganz T. The role of hepcidin in iron metabolism. Acta Haematol. 2009;122(2-3):78–86. doi:10.1159/000243791

[12] Enculescu M, Metzendorf C, Sparla R, et al. Modelling systemic iron regulation during dietary iron overload and acute inflammation: role of hepcidin-independent mechanisms. PLoS Comput Biol. 2017 Jan;13(1):e1005322. doi:10.1371/journal.pcbi.1005322

[13] Zhang H, Wang A, Shen G, et al. Hepcidin-induced reduction in iron content and PGC-1β expression negatively regulates osteoclast differentiation to play a protective role in postmenopausal osteoporosis. Aging. 2021;13(8):11296–11314. doi:10.18632/aging.202817

[14] Huang L, Liu Z, Liu H, et al. Biron overload impairs bone marrow mesenchymal stromal cells from higher-risk MDS patients by regulating the ROS-related Wnt/-catenin pathway. Stem Cells Int. 2020;2020:8855038.

[15] Pegg AE. The function of spermine. IUBMB Life. 2014 Jan;66(1):8–18. doi:10.1002/iub.1237

[16] Ramani D, De Bandt JP, Cynober L. Aliphatic polyamines in physiology and diseases. Clin Nutr. 2014 Feb;33(1):14–22. doi:10.1016/j.clnu.2013.09.019

[17] Lee H, Kim DH, Hwangbo H, et al. The protective effect of topical spermidine on dry eye disease with retinal damage induced by diesel particulate Matter2.5. Pharmaceutics. 2021 Sep 10;13(9):1–15.

[18] Jeong JW, Cha HJ, Han MH, et al. Spermidine protects against oxidative stress in inflammation models using macrophages and zebrafish. Biomol Ther. 2018 Mar 1;26(2):146–156. doi:10.4062/biomolther.2016.272

[19] Guidotti S, Facchini A, Platano D, et al. Enhanced osteoblastogenesis of adipose-derived stem cells on spermine delivery via β-catenin activation. Stem Cells Dev. 2013 May 15;22(10):1588–1601.

[20] Yamamoto T, Hinoi E, Fujita H, et al. The natural polyamines spermidine and spermine prevent bone loss through preferential disruption of osteoclastic activation in ovariectomized mice. Br J Pharmacol. 2012 Jun;166(3):1084–1096. doi:10.1111/j.1476-5381.2012.01856.x

[21] Tao Z, Tao M, Zhou M, et al. Niacin treatment prevents bone loss in iron overload osteoporotic rats via activation of SIRT1 signaling pathway. Chem Biol Interact. 2023 Dec 9;388:110827. doi:10.1016/j.cbi.2023.110827

[22] Tao ZS, Li TL, Wei S. Silymarin prevents iron overload induced bone loss by inhibiting oxidative stress in an ovariectomized animal model. Chem Biol Interact. 2022 Oct 1;366:110168.

[23] Singh S, Kumar R, Garg G, et al. Spermidine, a caloric restriction mimetic, provides neuroprotection against normal and D-galactose-induced oxidative stress and apoptosis through activation of autophagy in male rats during aging. Biogerontology. 2021 Feb;22(1):35–47.

[24] Tao ZS, Zhou WS, Yang M, et al. Resveratrol reverses the negative effect of alcohol on hydroxyapatite-coated implant osseointegration in senile female rats. Z Gerontol Geriatr. 2020 Oct;53(6):538–545. doi:10.1007/s00391-019-01595-3

[25] Tao ZS, Zhou WS, Xu HG, et al. Simvastatin can enhance the osseointegration of titanium rods in ovariectomized rats maintenance treatment with valproic acid. Biomed Pharmacother. 2020 Dec;132:110745.

[26] Tao Z, Zhou W, Zhang R, et al. Co-modification of calcium phosphate cement to achieve rapid bone regeneration in osteoporotic femoral condyle defect with lithium and aspirin. Am J Transl Res. 2021;13(3):952–966.

[27] Tao ZS, Zhou WS, Xu HG, et al. Aspirin modified strontium-doped beta-tricalcium phosphate can accelerate the healing of femoral metaphyseal defects in ovariectomized rats. Biomed Pharmacother. 2020 Dec;132:110911. doi:10.1016/j.biopha.2020.110911

[28] Tao Z, Li TL, Yang M, et al. Silibinin can promote bone regeneration of selenium hydrogel by reducing the oxidative stress pathway in ovariectomized rats. Calcif Tissue Int. 2022 June;110(6):723–735. doi:10.1007/s00223-021-00936-y

[29] Tao ZS, Li TL, Xu HG, et al. Hydrogel contained valproic acid accelerates bone-defect repair via activating notch signaling pathway in ovariectomized rats. J Mater Sci Mater Med. 2021 Dec 23;33(1):4.

[30] Li X, Lin H, Zhang X, et al. Notoginsenoside R1 attenuates oxidative stress-induced osteoblast dysfunction through JNK signalling pathway. J Cell Mol Med. 2021;25(24):11278–11289. doi:10.1111/jcmm.17054

[31] Gao Z, Chen Z, Xiong Z, et al. Ferroptosis - A new target of osteoporosis. Exp Gerontol. 2022 Aug;165:111836. doi:10.1016/j.exger.2022.111836

[32] Luo D, Ren H, Li T, et al. Rapamycin reduces severity of senile osteoporosis by activating osteocyte autophagy. Osteoporos Int. 2016 Mar;27(3):1093–1101.

[33] Pietschmann P, Skalicky M, Kneissel M, et al. Bone structure and metabolism in a rodent model of male senile osteoporosis. Exp Gerontol. 2007 Nov;42(11):1099–1108. doi:10.1016/j.exger.2007.08.008

[34] Ma H, Wang X, Zhang W, et al. Melatonin suppresses ferroptosis induced by high glucose via activation of the Nrf2/HO-1 signaling pathway in type 2 diabetic osteoporosis. Oxid Med Cell Longev. 2020;2020:9067610.

[35] Lei Y, Yang L, Ye C, et al. Involvement of intracellular and mitochondrial Aβ in the ameliorative effects of huperzine A against oligomeric Aβ42-induced injury in primary rat neurons. PLoS One. 2015;10(5):e0128366.

[36] He Z, Sun S, Waqas M, et al. Reduced TRMU expression increases the sensitivity of hair-cell-like HEI-OC-1 cells to neomycin damage in vitro. Sci Rep. 2016;6:29621. doi:10.1038/srep29621

[37] Zhang Y, Zhu X, Wang G, et al. Melatonin rescues the Ti particle-impaired osteogenic potential of bone marrow mesenchymal stem cells via the SIRT1/SOD2 signaling pathway. Calcif Tissue Int. 2020;107(5):474–488. doi:10.1007/s00223-020-00741-z

[38] Deng Z, Wang Z, Jin J, et al. SIRT1 protects osteoblasts against particle-induced inflammatory responses and apoptosis in aseptic prosthesis loosening. Acta Biomater. 2017;49:541–554. doi:10.1016/j.actbio.2016.11.051